Reflective solar band striping mitigation method for the GOES-R series advanced baseline imager using special scans

Monica Cook,[a,*] Francis Padula,[a] Dave Pogorzala,[b] Aaron Pearlman,[a] Joel McCorkel,[c] and Alexander Krimchansky[c]

[a]GeoThinkTank LLC, Washington, DC, United States
[b]Centauri, Chantilly, Virginia, United States
[c]NASA Goddard Space Flight Center, Greenbelt, Maryland, United States

Abstract. The large focal plane arrays used in the new generation of the Geostationary Operational Environmental Satellites (GOES) advanced baseline imager (ABI) introduce new calibration challenges compared with the heritage GOES imagers. The increased number of detectors allows for increased spatial, spectral, and temporal performance, but as a trade-off, it has an increased risk of image striping. We detail the development of a new postlaunch relative calibration capability for ABI reflective solar bands that utilizes ABI special scans to generate a set of relative gains that can be applied to improve image quality and reduce image striping. Results demonstrate that the method reduces image striping in the ABI solar reflective bands over varying scene content and time, both diurnally and over an extended period. This methodology ensures a calibration strategy that is consistent with heritage approaches yet adapts to the new postlaunch validation challenges presented by the new class of operational imagers in the GOES-R series. The developed approach is ready for operational use, as needed, and can be easily implemented into operations to support the operational production of geostationary imagery of the Earth. © *2020 Society of Photo-Optical Instrumentation Engineers (SPIE)* [DOI: 10.1117/1.JRS.14.032409]

Keywords: relative calibration; reflective solar bands; advanced baseline imager; special scans; image quality; image striping.

Paper 191027SS received Jan. 2, 2020; accepted for publication Jun. 16, 2020; published online Jun. 30, 2020.

1 Introduction

Advanced baseline imagers (ABIs) are the primary Earth observing sensors in the GOES-R series of instruments and operate on GOES-16 and GOES-17. These ABI instruments are the first two of four imagers planned in the GOES-R series. Compared with the heritage GOES imagers, the ABI has more spectral channels, increased spatial resolution, and increased temporal sampling. ABI has two scan mirrors, a north–south (N/S) scan mirror and an east–west (E/W) scan mirror, operating independently and simultaneously. ABI collects imagery in six reflective solar bands (RSBs) and ten thermal emissive bands (TEBs) using large focal plane arrays (FPAs), one for each channel, contained in three different focal plane modules (FPMs). Operationally, ABI uses on-board calibration targets (solar diffuser and blackbody target) combined with space views to produce a sensor specific absolute radiometric calibration traceable to the international radiometric scale (SI). This calibration is applied to the difference in detector digital counts between the Earth view and the space view to obtain the effective spectral radiance. For details regarding the ABI calibration algorithms and their implementation on the GOES-R ground segment, see Refs. 1 and 2, and a detailed overview of the ABI instrument and its operation can be found in Refs. 1–3. Analysis in this paper will focus on the RSB, as summarized in Table 1.

The large FPAs on ABI have substantially more detectors than the heritage GOES imagers that had between 2 and 8 detectors per channel (GOES O-P series). This increase in the number

*Address all correspondence to Monica Cook, E-mail: monica@geothinktank.com

1931-3195/2020/$28.00 © 2020 SPIE

Table 1 Channel characteristics for the RSB contained in the visible and near infrared FPM.[1]

Channel	Center wavelength (μm)	Nadir spatial resolution (km)
1	0.47	1
2	0.64	0.5
3	0.86	1
4	1.38	2
5	1.61	1
6	2.25	2

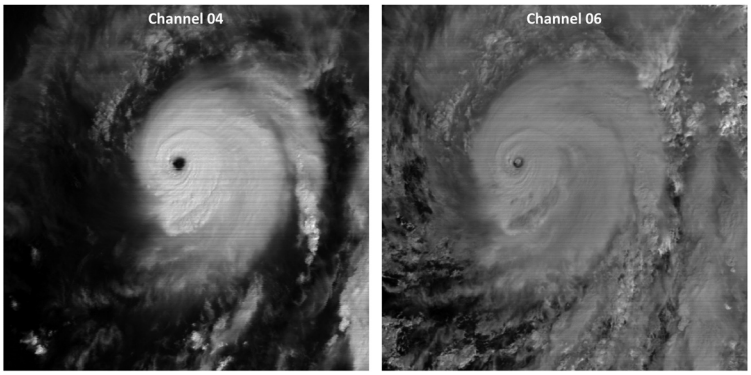

Fig. 1 Visible striping in images of hurricane Willa in the Pacific Ocean; GOES-17 ABI images from October 22, 2018, at 1700 UTC.

of detectors requires different methods to mitigate striping compared with those used in the heritage systems.[4] The ABI FPAs have three or six columns and a variable number of rows, between 332 and 1460, dependent upon channel; only one column per row is in use at any one time. The large number of detectors per channel leads to an increased risk of image striping due to potential detector-to-detector nonuniformity; one example of image striping in GOES-17 imagery is shown in Fig. 1. This variability in detector response has been observed and documented in many sensors that utilize focal planes containing hundreds to thousands of detectors and could be caused by a number of factors, including variation in manufacturing, temporal degradation, or variation of relative spectral response, among others.[5–7]

Space-based large FPA imaging systems were first introduced in the low-Earth orbit (LEO) pushbroom community. The swath width and image collection of pushbroom sensors in LEO are driven by the forward motion of the spacecraft, as shown in Fig. 2(a). High to moderate resolution LEO pushbroom imaging systems, which include instruments from QuickBird, RapidEye, and Landsat 8, among others, identified and operationally demonstrated a novel method to characterize variability in detector-to-detector response on-orbit by conducting a 90-deg yaw maneuver of the spacecraft to enable all detectors to collect over the same effective target area, referred to as a side-slither maneuver.[5–7,9,10] This maneuver provides an ideal method of on-orbit relative calibration or flat fielding as it enables the large swath width of the FPAs to be constrained to a much smaller area, effectively the size of its projected FPA width (and any FPA misalignment issues); this is illustrated in Fig. 2(b).[8] This approach has been used operationally[5–7,9] for relative on-orbit calibration and/or image striping mitigation of LEO pushbroom instruments and enables postlaunch image quality performance mitigation capabilities to address some of the challenges of detector-to-detector uniformity in large FPAs on-orbit.

ABI can utilize its scan flexibility to apply the same technique from geostationary orbit but without the need for a special maneuver. The scan flexibility of the ABI from its two scan mirrors

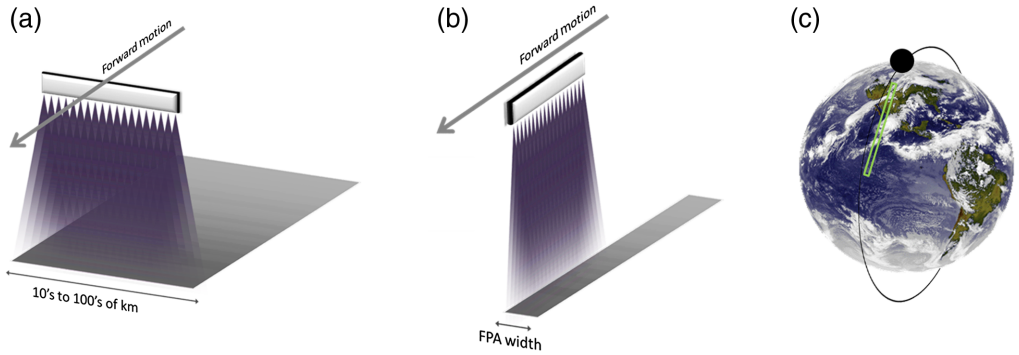

Fig. 2 (a) Illustration of the focal plane motion and image swath during nominal collection of a pushbroom sensor.[8] (b) Illustration of the focal plane motion and image swath during side-slither collection of a pushbroom sensor.[8] (c) Illustration of the focal plane motion and image swath during side-slither collection in LEO.

enables customizable special scans that can be used in support of mission operations. One such special scan is the north–south scan (NSS), an equivalent acquisition to the LEO side-slither collections without requiring a spacecraft maneuver. In nominal ABI scanning mode, the full disk image is captured in 22 horizontal swaths, with an effective swath width of ~500 km in the north–south direction, as illustrated in Figs. 3(a) and 3(b). In a single swath of nominal scanning mode, motion of the E/W scan mirror sweeps from west to east, while the N/S scan mirror is stationary. The ABI NSS is notionally achieved by holding the E/W scan mirror fixed and moving the N/S scan mirror; though in practice, both E/W and N/S mirrors are moved to ensure that a true north–south footprint is collected, as illustrated in Figs. 3(c) and 3(d). To acquire all 16 bands over the same validation target, which takes only tens of seconds to complete, 16 unique NSSs are required using a unique incremental shift in the E/W scan mirror to position a given band's FPA over the desired target location before each NSS. Because each channel provides

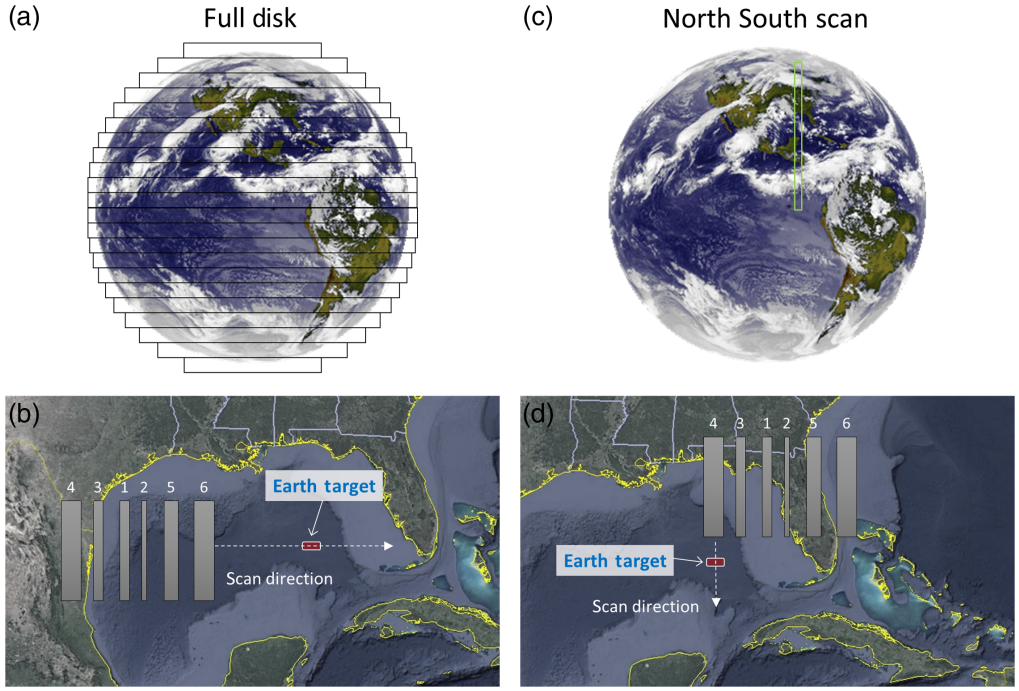

Fig. 3 (a) Illustration of the horizontal swaths in full disk collection. (b) Graphical illustration (not physical) of the motion of the FPAs during nominal collection. (c) Illustration of the vertical swath of a NSS. (d) Graphical illustration (not physical) of the motion of the FPAs during NSS collection. Note that the white numbers denote the channel for each FPA; only RSB are illustrated.

data for every scan, 16 unique scans result in 256 NSSs. There is a portion of the NSS data where every detector in every channel has collected the same effective location on the Earth, the overlap region, which is the data of interest to this effort and will be discussed further in Sec. 2.3.

Again, the effective swath width (north to south extent) of a nominal ABI scan is ~500 km. The primary RSB Earth calibration/validation targets accessible from the GOES East and GOES West positions are the Uyuni Salt Flats in Bolivia (GOES East only) and the Sonoran Desert, which are ~100 km × 100 km and 120 km × 60 km, respectively, with only a portion of each area being uniform enough to use for calibration. Note that both are significantly smaller than the swath width that would be required for all detectors to image a uniform area in nominal scanning mode. Because of the nature of the NSS collection mode, the area of the calibration/validation target need only be as large as one detector in the north to south direction and three to six columns in the east to west direction. This could be as small as 0.5 km × 1.5 km or as large as 2 km × 12 km, depending on the channel, looking nadir at the subsatellite point of the instrument. Operationally, a customized scan mode, referred to as Timeline 25, was developed initially for the GOES-16 postlaunch validation airborne science field campaign,[11,12] which evokes this NSS collection strategy and enables repeats of each channel to be collected. Timeline 25 repeatedly collects NSSs of the target of interest for all channels throughout the 5-min duration of the timeline, in addition to Meso collections and the necessary housekeeping collections such as blackbody images for IR calibration, space looks, and star looks. This results in five repeats of the NSS of the target of interest for channels 1 to 3 and four repeats of the target of interest for channels 4 to 16. This operational scan mode is used to collect the data for the analysis below.

The focus of the postlaunch relative calibration capability discussed in this work is to address detector-to-detector nonuniformity, in the ABI RSB, that is not captured in the operational radiometric calibration. This paper will demonstrate a new postlaunch capability that leverages the successes of a technique used for LEO large FPA; this technique is adapted and applied to large FPA in geostationary orbit using NSSs to achieve image striping mitigation and improved image quality. Results will show that this relative calibration approach can be applied operationally, and therefore improve image quality, to all collections of varying scene content and time, both diurnally and over an extended period. This will be demonstrated on GOES-17; though it is applicable to all ABI. Finally, a brief discussion will summarize the operational readiness of the approach.

2 Methodology

This section will discuss the elements of the approach, which include tasking the ABI NSS image collections, NSS data processing and analysis, generation of ABI relative gains, application of the relative gains to ABI calibrated and navigated radiance data, and qualitative and quantitative performance evaluation of striping mitigation and image quality improvements. As a reference, ABI Level 0 (L0) data are down-linked to the ground station, converted to Level 1 beta (L1β) calibrated and geolocated data, and then resampled to a fixed grid coordinate system, referred to as Level 1b (L1b) data.[1,2] The ABI L0 NSS data are not processed through the ground station but are processed offline using the GOES-R ABI Trending and Data Analysis Toolkit to convert the L0 NSS collection data to L1β data that is required for this method. Data for this method are calibrated and geolocated but not resampled to the fixed grid.

2.1 *Overview of On-Orbit Relative Calibration Using ABI NSS Data*

The ABI NSS-based relative calibration ("flat fielding") approach can be briefly summarized in five basic steps, shown in Fig. 4. First, all detectors, for each RSB channel, need to image the same uniform source with a NSS special collection; examples of a uniform source (referred to here as a validation target) are the desert, the ocean, the moon, or a uniform cloud. This collection is acquired using Timeline 25. The special collection data are then processed to L1β (calibrated and geolocated) radiance data, analyzed, and used to generate a relative gain value for each detector in each channel using data selected over the validation target of interest. The computed

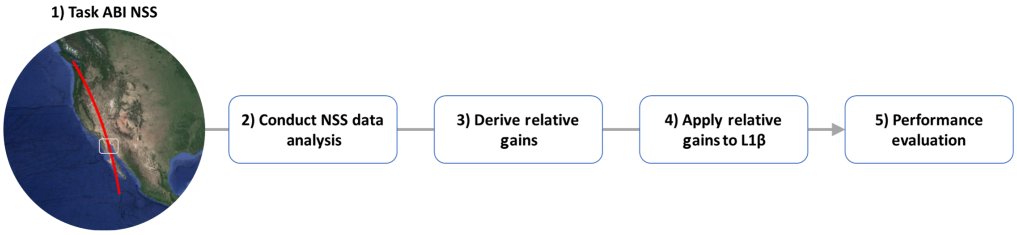

Fig. 4 The postlaunch relative calibration capability can be summarized in five steps: (1) task ABI NSS collection of uniform Earth target(s), (2) conduct NSS data analysis over the validation target, (3) derive relative gains from the NSS data, (4) apply relative gains to L1β image data (nominal collection), and (5) conduct performance evaluation to ensure data quality.

relative gain values are then applied to the nominal collection L1β image data; this step is also referred to as destriping. A qualitative and quantitative performance evaluation is conducted on the resulting L1β imagery to ensure data quality.

The application of relative gains derived from this method can result in reduced image striping and improved image quality by reducing the detector-to-detector nonuniformity as a result of all detectors being normalized by the average response to the "same radiance" across the entire FPA. This approach is dependent upon the assumption that the source is "uniform" so that all detectors, of a given channel, view the same radiance; thus multiple NSS validation targets are collected in practice to ensure the quality of input data. Note that the average of the relative gain values for any one channel is equal to one. Therefore, when applied to an image, the mean radiance value of the image is unchanged. This is significant because it establishes that the application of this relative calibration approach maintains the absolute radiometric calibration of the instrument while improving image quality through the reduction of detector-to-detector variability in each channel.

2.2 *NSS Data Collection for Relative Gain Computation*

NSSs, collected using Timeline 25 as described in Sec. 1, can be automatically scheduled to collect a fixed target location, such as a desert validation site, or dynamically tasked to collect a variety of targets in real time. The ABI NSSs used in this work were dynamically tasked to collect targets of interest for on-orbit detector-level relative gain generation and radiometric performance characterization of the system. Each NSS data collection using dynamic tasking requires a well-coordinated line of communication between the calibration science team and mission operations personnel during tasking and collection. The calibration scientist(s) identify potential NSS targets of interest, specified by latitude and longitude coordinates, using real-time ABI L1b full disk imagery within an Advanced Weather Interactive Processing System (AWIPS) workstation. The identified NSS Earth target locations of large desert(s), cloud free ocean, and/or large uniform clouds are passed to mission operations for NSS collection in pseudo-real time. A variety of targets with a range of radiance values are collected to improve system characterization capabilities and include designed redundancy in the event of nonuniformities in the collected scene. This concept of operations is robust and has been successfully executed in the postlaunch testing of GOES-16 and GOES-17.

2.3 *NSS Data Analysis*

The NSS data are processed offline, not by the ground segment, and analysis is conducted at the L1β data level. L1β data are both calibrated and geolocated, meaning that every pixel has a radiance value and a location on the Earth.[1] Although the analysis and results in Sec. 3 utilize NSSs of only uniform cloud targets, a NSS collection of the Sonoran Desert will be used here to illustrate the processing of NSS data as the desert/ocean boundary provides a unique case to demonstrate and easily interpret the data. A visualization of a single channel of a NSS is provided in Fig. 5(a). A typical NSS swath is ~2000 km in length and between 1.5 and 12 km in width at nadir, dependent on the number of detector columns for each channel. The desired functionality

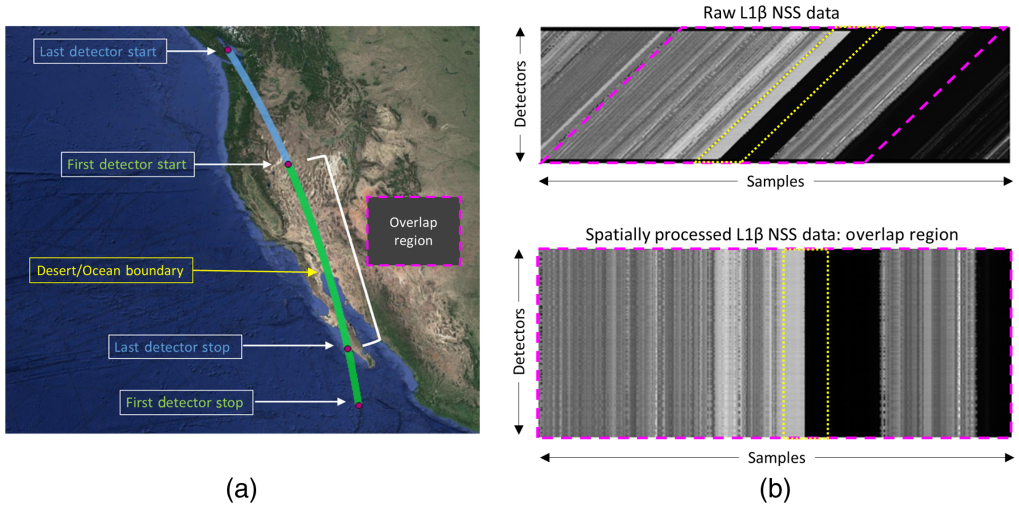

Fig. 5 (a) Illustration of the location of a NSS on the Earth and how to identify the overlap region; the NSS overlap region is the region encompassing all detectors viewing the same location on the earth. (b) Grayscale representation of the NSS radiance data [W/(m^2 sr μm)]; channel 3 data (676 detectors in channel 3[1]) from GOES-17 collected on August 6, 2018, at 1900 UTC is shown as an example. For reference, samples collected from north to south are displayed left to right. Top: the raw L1β NSS radiance data for the entire scan with the overlap region highlighted in a dashed magenta line and the desert/ocean boundary highlighted in a dotted yellow line. Bottom: spatially processed L1β radiance data for the overlap region only that optimizes the dataset for analysis.

of the collection resides in the overlap region—the region bounded by the starting point of the first detector and the ending point of the last detector—which has been collected by all of the detectors. The overlap region is approximately between 650 and 1100 km in length; the length of the scan is dependent on the number of detectors per channel. Collection is designed to ensure the overlap region includes the validation targets of interest. The top image in Fig. 5(b) shows a grayscale representation of the raw ABI NSS L1β radiance data; showing channel 3 as an example, this displays the highest radiance values as white and the lowest radiance value as black, with all other values scaled in between. Each row illustrates the spatial–temporal radiance samples from a single detector during the NSS collection; the dashed magenta box illustrates the overlap region. The slanted lines in the image represent the same location on the Earth viewed by all detectors; the slant results from each detector collecting the same location consecutively, rather than simultaneously. In this example, the boundary between the high-radiance values of the desert and the low-radiance values of the ocean is clearly evident in the middle of the overlap region, as shown by the distinct white/black edge that is emphasized by the dotted yellow line. The bottom image in Fig. 5(b) illustrates L1β NSS radiance data from only within the overlap region that have been spatially processed to optimize the dataset for analysis; each column represents the same location on the Earth viewed by all detectors. The degree of homogeneity observed in each column represents the level of detector-to-detector uniformity from the scene. Notice that in Fig. 5(b) the small variations in detector response versus location are evident in the dataset. More details on processing and sampling NSS data can be found in Ref. 13. For this analysis, NSS data processing will focus solely on the NSS overlap region. Once the overlap region has been identified, the data are ready to be analyzed for the relative gain generation for each channel.

2.3.1 *ROI selection*

To generate a set of relative gains, a spatially uniform region of interest (ROI) in the overlap region with high-radiance values is desired to increase the signal-to-noise ratio of the input dataset.[5] In practice, the ROI is selected manually to include as many samples as possible while maintaining spatial uniformity. To optimize the spatial uniformity, this could be as small as one detector in the north to south direction, requiring a spatially uniform area ranging from 0.5 km $\times$ 1.5 km to 2 km $\times$ 12 km, depending on the channel being processed. To optimize

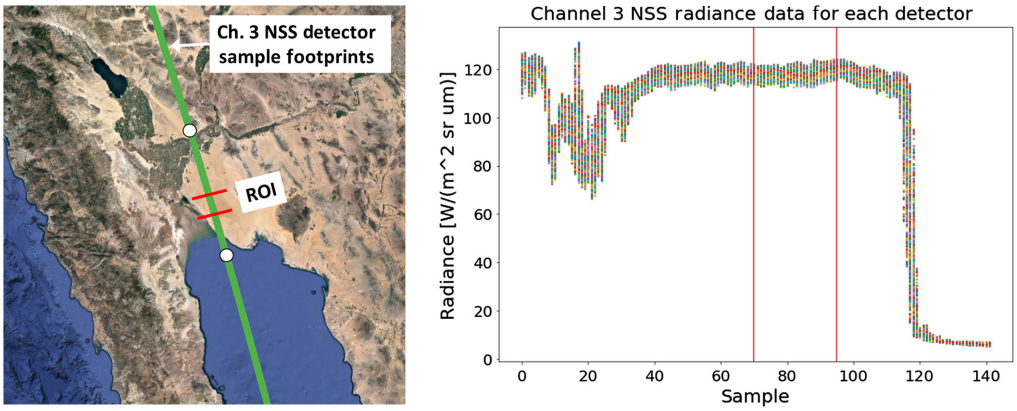

Fig. 6 (a) A map illustrating the detector sample footprints of GOES-17 ABI Channel 3 NSS data collected August 6, 2018, at 1900 UTC targeting the Sonoran Desert. The circles in (a) denote the extent of the data plotted in (b); each channel 3 detector is represented by a different color in the plot. The lines in (a) denote the extent of the ROI, shown in (b) by the vertical red lines. The location of the ROI is selected to include as many samples as possible with high uniform radiance.

signal to noise, this could be as large as the entire overlap region, with a maximum spatial extent of ∼650 to ∼1100 km, dependent upon the channel. The ROI is selected manually, sometimes as an iterative process, based on a qualitative evaluation of both the L1β data from the NSS and the relative gains that are generated. The resulting ROI, used in further processing, is often found at or near the location of the collection target (desert, ocean, or cloud), since this region was predetermined—"targeted." Since the ABI FPAs consist of multiple columns per channel, each of the columns collects a slightly different location on the Earth, shown by the width of the green line in Fig. 6(a). Thus well planned targeting, which includes prior analysis conducted to ensure the validity of a given target, and careful selection of a spatially uniform ROI using the criteria described above aid in the mitigation of potential discontinuities as a result of scene content in the generation of relative gains.

Figure 6(b) illustrates another fundamental view of NSS data to characterize the detector-level performance of each channel. The same NSS collection of the Sonora Desert illustrated in Fig. 5 is also shown in Fig. 6. In Fig. 6(b), each sample is a single location on the earth and each detector is plotted in a different color; note that the desert/ocean boundary is clearly evident around sample ∼120, where the radiance values significantly decrease. If all detectors responded equivalently to the same radiance, all points per sample in this plot would overlay on one-another. Therefore, any observed variability in the y axis at each sample location illustrates detector-to-detector nonuniformities present in the data. This view is the primary tool to select the ROI. The data within the ROI, illustrated in Fig. 6(a) and by the red vertical lines in Fig. 6(b), are the data used to generate relative gains for further analysis.

2.4 *Generation and Application of Relative Gains for Striping Mitigation*

Only the data from within the selected ROI are used to generate a relative gain value for each detector in each channel using Eq. (1).[5,6] The relative gains ($g_{\mathrm{rel,ch},i}$) are generated by dividing the detector average radiance ($\overline{L_i}$) by the channel average radiance ($\overline{L_{\mathrm{ch}}}$):

$$g_{\mathrm{rel,ch},i} = \frac{\overline{L_i}}{\overline{L_{\mathrm{ch}}}}. \tag{1}$$

The computed relative gain values are then applied to the nominal collection image data (L1β) using Eq. (2); this process is also referred to as destriping. The destriped imagery ($L_{\mathrm{destriped},i}$) is calculated in Eq. (2) by dividing the L1β values for each detector ($L_{\beta,i}$) by the relative gain value for that specific detector ($g_{\mathrm{rel,ch},i}$) for each given channel:

$$L_{\text{destriped},i} = \frac{L_{\beta,i}}{g_{\text{rel,ch},i}}. \tag{2}$$

The mean value of the relative gains for any one channel is equal to 1; therefore, when the relative gains are applied to an image, the mean radiance value of the image is unchanged, but the striping in the imagery should be reduced and the image quality improved. For clarity, the application of this relative calibration approach maintains the absolute radiometric calibration of the instrument while improving image quality through the reduction of detector-to-detector variability in each channel.

2.5 *Qualitative and Quantitative Evaluation*

Image quality impacts as a result of the relative calibration methodology can be evaluated qualitatively by visually comparing the original L1β imagery with the L1β imagery with relative gains applied; the L1β imagery with relative gains applied is also referred to as destriped imagery. The effectiveness of this qualitative evaluation is dependent on the display and scene content of the image. Although improved image quality was often evident, a method to quantitatively evaluate the effects of the striping mitigation strategy was also desired. An image streaking metric from Ref. 5 is shown in Eq. (3); $\overline{Q_i}$ is the detector average radiance, and S_i is the resulting streaking metric, referred to as the streaking metric ratio:

$$S_i = \frac{|\overline{Q_i} - \frac{1}{2}(\overline{Q_{i-1}} - \overline{Q_{i+1}})|}{\overline{Q_i}}. \tag{3}$$

This calculation results in one streaking metric ratio value per row—a row being a single detector of a given channel—in the image being evaluated. Streaking metric ratio values for both original and destriped imagery of various scene contents and various relative gain sets were investigated to characterize the magnitude of the streaking metric ratio values as it relates to image quality. Overall, a reduction in the streaking metric ratio value was found to correspond to improved image quality based on the visual evaluation; one example is illustrated in Fig. 7. Figure 7(a) shows the original L1β imagery, Fig. 7(b) shows the destriped imagery, and Fig. 7(c) shows a plot representing the streaking metric ratio value for each row of the original and destriped images.

To evaluate the relative calibration methodology on a large number of scenes with varying parameters such as scene content and image acquisition time, a performance metric that is the average streaking metric ratio value for all rows in a single image as shown in Fig. 7(d) was established; it is referred to as the average streaking metric ratio or just the streaking metric. By having a single streaking metric value for each scene, the reduction in striping for larger datasets over different spatial and temporal extents could be characterized. Simply stated, higher average values of the streaking metric corresponded to lower image quality and lower average values of the streaking metric corresponded to higher image quality, as shown in Fig. 7. For the sake of brevity in this work, results from other channels have been omitted, but all were found to have consistent performance via qualitative and quantitative image striping evaluation. This streaking metric is used for evaluation in the results presented below.

In summary, the fundamentals of the relative calibration methodology using ABI special scans have been established. The results presented below are intended to demonstrate the performance of the approach for varying scene content and imagery collected throughout the day and over an extended period of time.

3 Results

Relative gains for this work were generated from a collection of NSS data that was actively tasked using the approach described in Sec. 2.2. After an initial validation of the methodology, the goal of this analysis was to illustrate that this relative calibration approach can be applied operationally, and therefore improve image quality, to all collections of varying scene content acquired throughout the day and over an extended period of time. This section will showcase

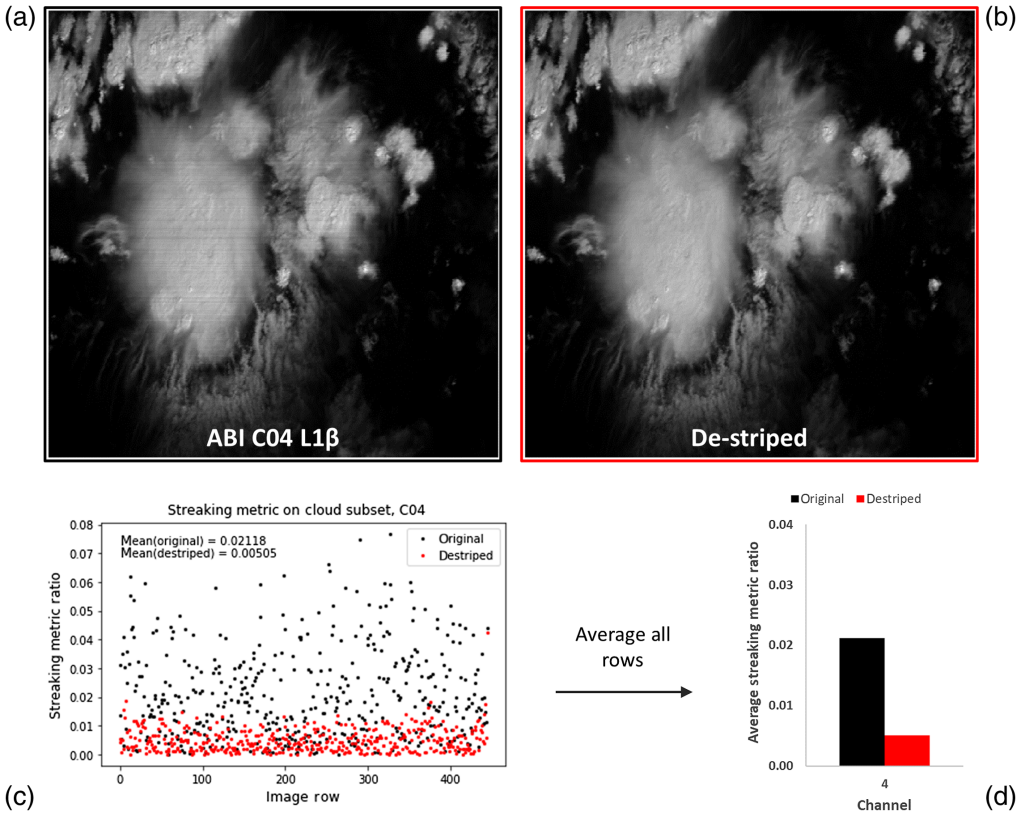

Fig. 7 The image quality can be evaluated qualitatively by comparing original and destriped L1β imagery as shown in (a) and (b). Streaking metric ratio [Eq. (3)] values for each row of the images are plotted in (c). Averaging all rows in a single image generates a single quantitative metric, as shown in (d). Note that a higher average corresponds to lower image quality and a lower average corresponds to higher image quality. This image subset was collected by GOES-17 ABI on December 7, 2018, at 2040 UTC.

the process and the results produced from the NSS collections and illustrate the image quality improvements for a variety of scenes using the qualitative and quantitative metrics discussed above.

3.1 *NSS Data Collection*

This work focuses on three consecutive NSS data collections acquired on December 6, 2018. The NSSs were actively tasked to collect three unique uniform cloud targets at varying radiance levels using the process described in Sec. 2.2. A summary of the data collection is shown in Table 2; the approximate location of each NSS over the uniform cloud is illustrated with the first full disk image captured immediately after the consecutive NSS acquisitions in Fig. 8.

Table 2 Summary of the times and locations of the NSSs collected during active tasking on December 6, 2018. Only data from the 2030 UTC and 2040 UTC acquisition times will be included in the following results.

Sensor	Collection	Date	Time (UTC)	Location (°N, °W)
GOES-17 ABI	NSS	December 6, 2018	2030	−13.69, −145.93
GOES-17 ABI	NSS	December 6, 2018	2035	7.18, −171.25
GOES-17 ABI	NSS	December 6, 2018	2040	47, −144.31

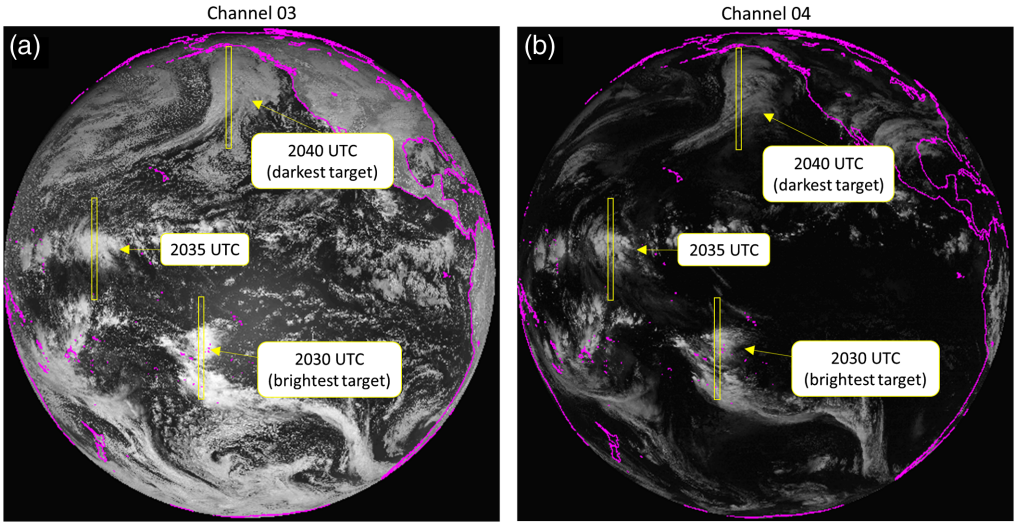

Fig. 8 An illustration of the approximate location and the uniform cloud collected for each NSS acquisition from GOES-17 on December 6, 2018 (details included in Table 2), shown in channel 3 (a) and channel 4 (b) of the full disk image collected immediately following the NSS acquisitions. Images courtesy of Ref. 14.

The remainder of the analysis of this work will focus on the NSS data from the 2030 UTC and 2040 UTC collections.

3.2 *Relative Gains*

The ROI for each NSS collection considered in this effort (collections at 2030 UTC and 2040 UTC) was determined by including as many samples as possible for a contiguous region that showed both the highest possible radiance and maintained uniformity. This is identified by considering regions that are both high in radiance value and flat among the majority of detectors in the radiance versus sample plots shown in Figs. 9(b) and 9(c). Note that the same ROI location and spatial extent is used for every channel. Using Eq. (1), relative gains were produced for each channel. Figure 9 illustrates for the two separate Timeline 25 collections, using channel 4 as an example, the relative gains derived for each dataset [Fig. 9(a)], the raw NSS L1β data [Fig. 9(b)], and the relative gain correction applied to the NSS radiance datasets [Fig. 9(c)]. The ROIs used to generate the relative gains for each collection are indicated by the two gray vertical lines in Figs. 9(b) and 9(c). After applying the relative gains to the radiance data from which they were generated, the detector variability was reduced in both sets of data, as expected. This is a good check to ensure correction implementation.

For clarity, in an ideal case, all detectors would respond equivalently to the same radiance, meaning that in Fig. 9(b), where each detector is plotted in a different color, all points per sample would overlay. Thus any observed variability in the y axis at each sample location illustrates detector-to-detector nonuniformities. Through the application of the relative gain correction using Eq. (2), the results in Fig. 9(c) show that the detector-to-detector nonuniformity has improved. In both sets of data, the detector-to-detector variability was reduced, but the reduction is especially evident in the 2030 UTC dataset at higher radiance levels; more detector-level discontinuities were observed with higher scene radiance.

3.3 *Image Striping Mitigation in ABI RSB*

Both sets of relative gains for all RSB described in Sec. 3.2 were applied to a subset of a full disk image acquired on December 7, 2018, at 2040 UTC, one day after the NSS acquisitions. The subset domain was selected for ease of processing and consisted of five swaths just north of the equator that contain fundamental scene content (land, ocean, and clouds) of the full disk imagery.

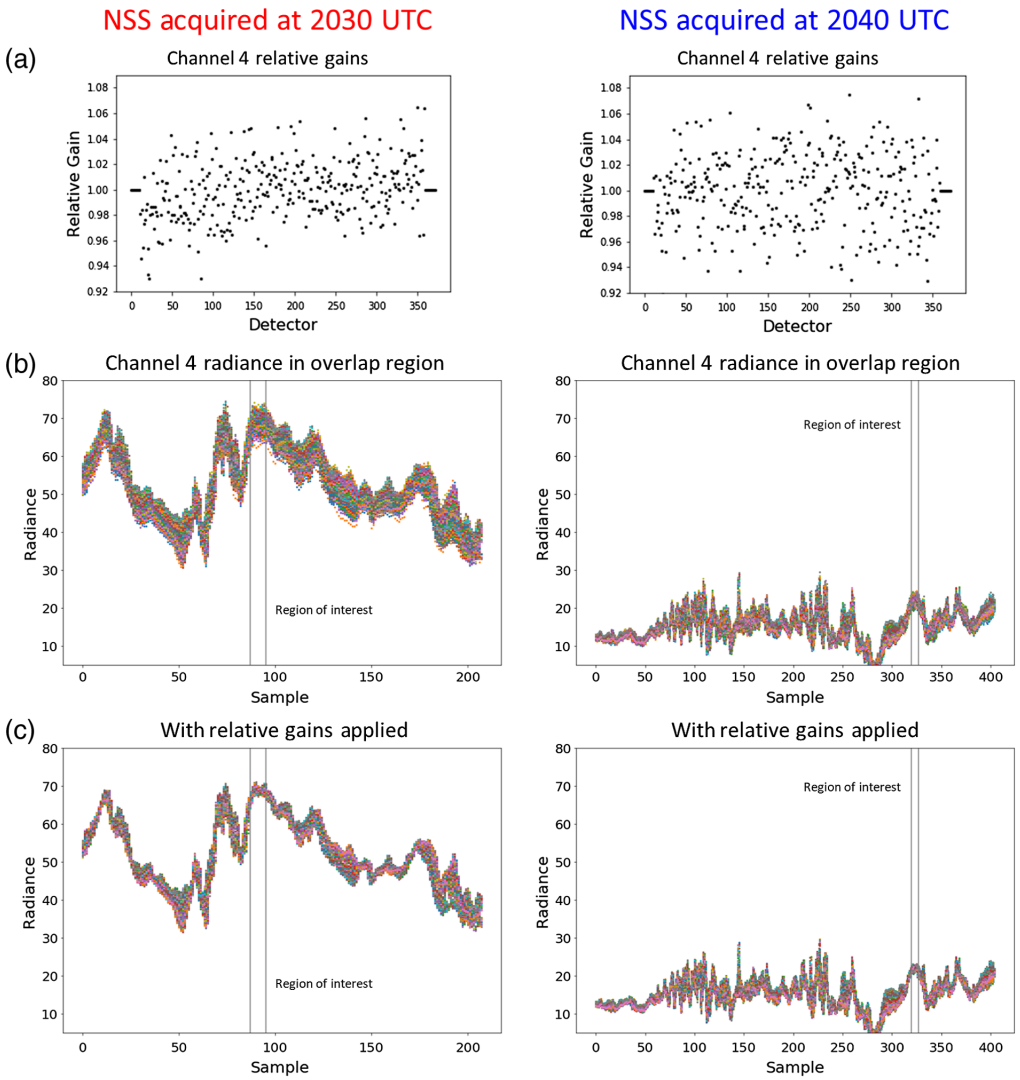

Fig. 9 (a) Relative gains derived from two Timeline 25 collections from GOES-17 on December 6, 2018, acquired at 2030 UTC (left) and 2040 UTC (right); details of these acquisitions are given in Table 2. Channel 4 is shown as an example. A graphical representation of a portion of the channel 4 radiance data [W/(m^2 sr μm)] from within the overlap region for the two collections is shown—the L1β radiance data in (b) and the same radiance data after the relative gains were applied in (c). Each detector is plotted as a different color. The ROI used to generate the relative gains, selected manually for uniformity and brightness, is illustrated by the gray vertical lines.

The streaking metric was calculated on the original L1β subset domain and for the same subset domain with each set of relative gains applied to assess image quality performance. The streaking metric results are illustrated in Fig. 10 and demonstrate that the relative calibration approach improves image quality.

Notice in Fig. 10 that the relative gains generated from the NSS acquired at 2030 UTC have a greater impact on reducing striping in channels 4, 5, and 6 than the relative gains generated from the NSS acquired at 2040 UTC. The opposite is true for channels 1, 2, and 3. Both sets of relative gains were applied to all of the imagery included in these results, and this pattern was found to be consistent. The root cause of this finding remains an open research item; however, the important finding is that an optimal set of relative gains that improves image quality for all bands can be identified. Only results for this optimal set of gains will be illustrated for the remainder of the analysis. The performance analysis highlighted here represents a practical approach for the identification of an optimal set of relative gains for potential operational use.

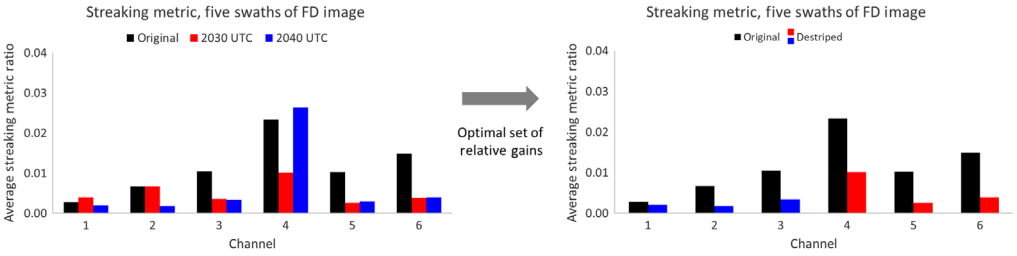

Fig. 10 Streaking metric results for the subset domain of a full disk image acquired with GOES-17 ABI on December 7, 2018, at 2040 UTC, one day following the NSS acquisition, with and without relative gains applied. Black represents the streaking metric values for the original L1β imagery. Red represents the streaking metric values for the same scene after relative gains generated from the NSS acquired at 2030 UTC were applied. Blue represents the streaking metric values for the same scene after relative gains generated from the NSS acquired at 2040 UTC were applied. Note that an optimal set of relative gains has been identified that improves image quality in all bands.

3.4 *Spatial Performance Evaluation*

It is important to consider the effects of relative gains for all scene content, including that which is difficult to analyze visually. Therefore, cloud, land, and ocean subsets were selected for evaluation; these images are shown in Fig. 11, and streaking metric results after application of the optimal set of relative gains are shown in Fig. 12. Results found that the relative calibration approach was consistent across all scene types in improving quality.

For the sake of brevity, only the quantitative analysis is shown here; however, both qualitative and quantitative analyses were conducted on the data and consistent results were found across all bands. As shown in Fig. 12, the optimal set of relative gains reduces image striping consistently for all channels. There are two special cases to consider. The first is channel 1; qualitative and quantitative analyses show that there is less image striping in channel 1 than all other channels. Therefore, application of relative gains has little or no effect on this channel because the striping is already low. The second special case is the ocean subset image. Using the methodology described in Sec. 2.5, if even one row in the scene has very low or close to zero radiance values, the streaking metric value for the scene can become quite large, as illustrated in Fig. 12(b).

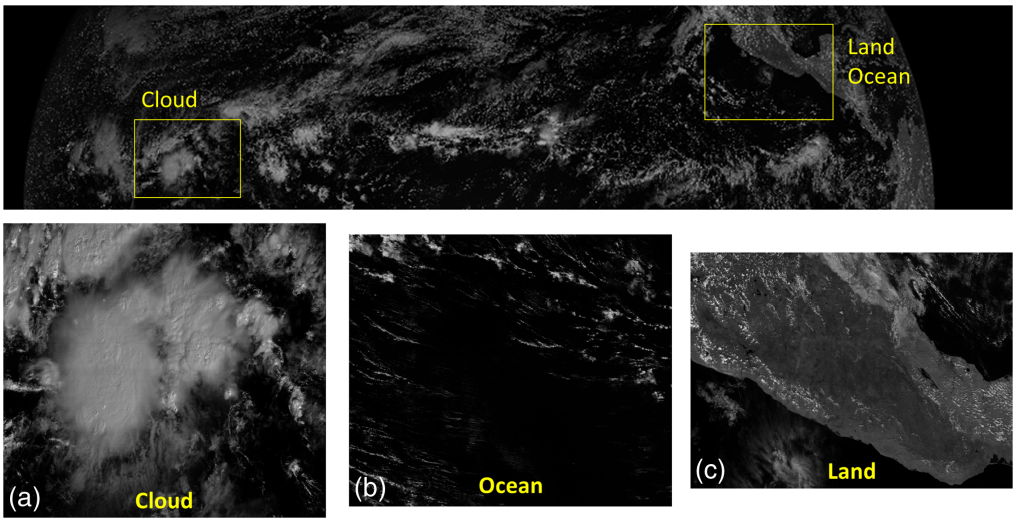

Fig. 11 (a) Cloud, (b) ocean, and (c) land subsets selected from the subset domain of the full disk image collected from GOES-17 ABI on December 7, 2018, at 2040 UTC; a grayscale representation of channel 3 is shown.

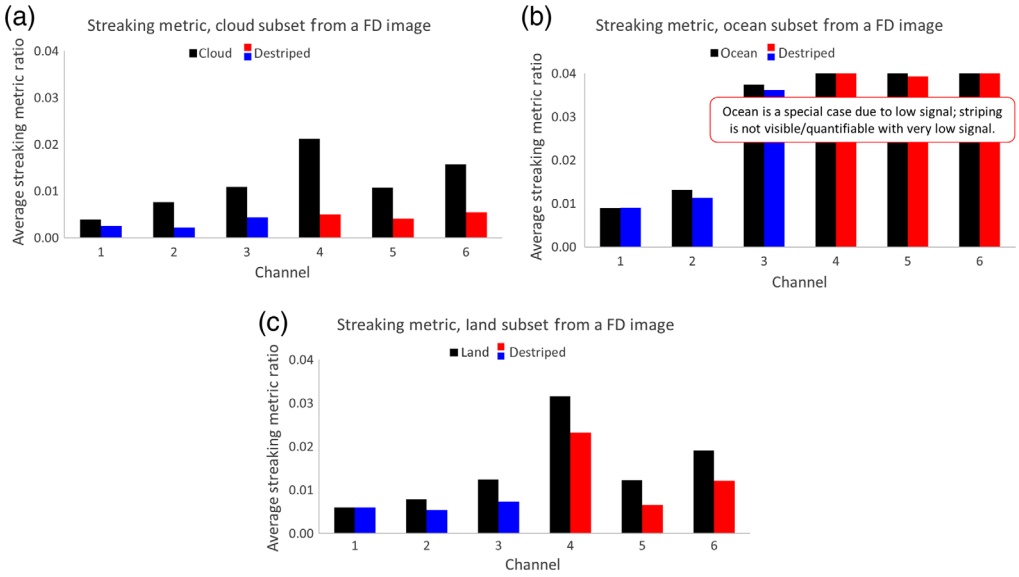

Fig. 12 Streaking metric results for (a) cloud, (b) ocean, and (c) land subset images shown in Figs. 11(a), 11(b), and 11(c), respectively.

It was found that the streaking metric is not applicable in the evaluation of scenes with low or close to zero signal. With these special cases accounted for, we can conclude that the application of the optimal set of relative gains reduces image striping over all scene content evaluated in this effort.

3.5 *Diurnal Performance Evaluation*

Thus far, all results have been shown for images captured at approximately the same time of day as the NSS acquisitions with an almost fully illuminated full disk image. It is important to consider the effects of the striping mitigation strategy throughout the day; this accounts for changes in scene illumination and instrument performance over a short period of time. The optimal set of relative gains was applied to the same subset domain from one full disk image per hour for 24 h. Note that only images with solar reflected light were included in the analysis below; the analysis includes images from December 7, 2018, at 1230 UTC to December 8, 2018, at 0530 UTC. The streaking metric evaluation of these images for all channels is shown in Fig. 13. This approach assumes that the diurnal performance of a given day is largely representative of any day. This assumption is consistent with our understanding of the system performance at this time. Results found that the relative calibration approach was consistent in improving quality throughout the day in all channels.

In all channels, the application of relative gains demonstrated improved image quality that was shown to be consistent over the diurnal cycle. Improvements were especially evident in channels 2 to 6. Similar to the spatial results discussed in Sec. 3.4, the application of relative gains to channel 1 imagery has little or no effect on image striping due to the low detector-to-detector variability in the original image. Also, channel 4 imagery has low or zero signal when there are no clouds, similar to the ocean subset shown in Fig. 12. This quantitative metric has limitations when portions of the scene have low or zero signal. Therefore, particularly in images where the full disk is partially or slightly illuminated, the streaking metric can become very large because it is calculated with a large amount of dark imagery. This is not an indication that the relative calibration method was ineffective but that there was a limitation in the quantitative evaluation for these scenes. Note that the qualitative analysis shows that striping in the cloud regions was mitigated in channel 4. With these special cases accounted for, we can conclude that the application of the optimal set of relative gains reduces image striping over all hours of the day.

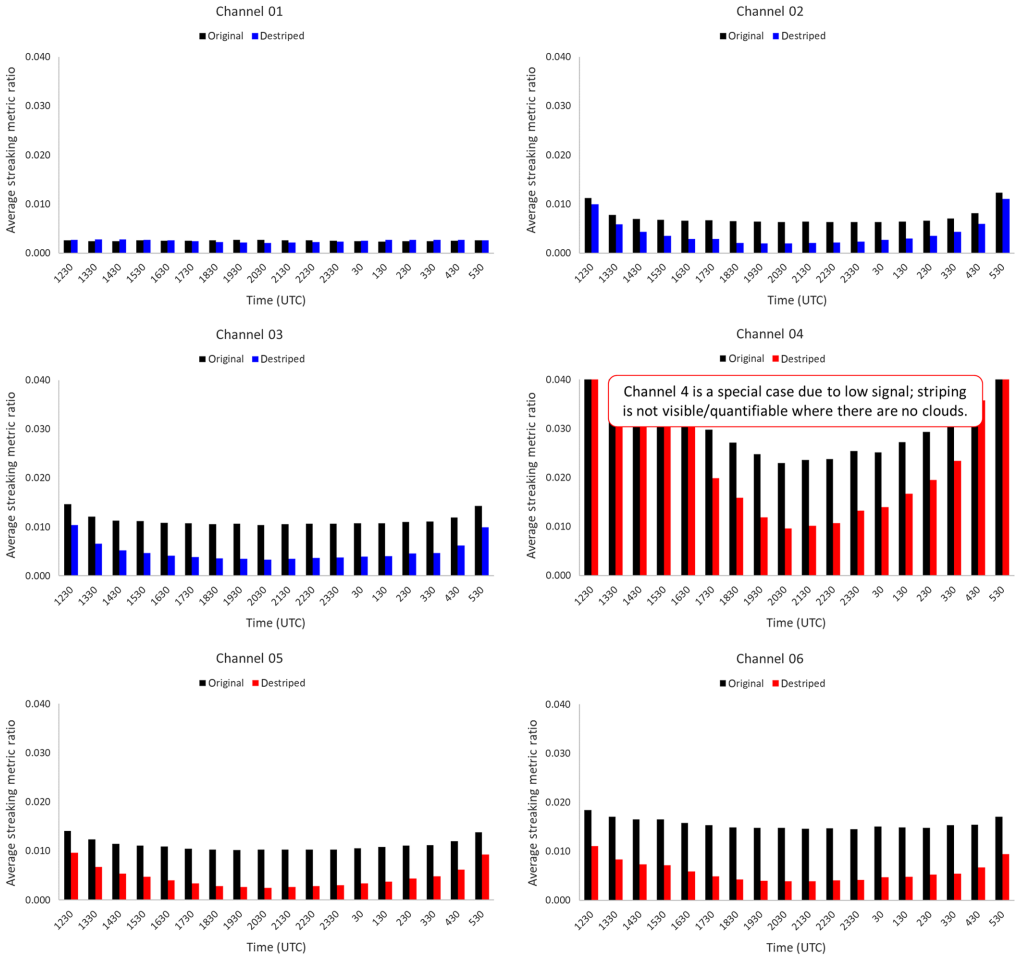

Fig. 13 Streaking metric results for the subset domain of one full disk image per hour from December 7, 2018, at 1230 UTC to December 8, 2018, at 0530 UTC. This illustrates the ability to successfully apply relative gains to all scenes that have solar illumination.

3.6 *Extended Temporal Performance Evaluation*

The striping mitigation strategy will now be investigated over an extended period of 5 months to account for seasonal changes in illumination and instrument behavior over time. The streaking metric was evaluated on the subset domain of a full disk image captured at 2030 UTC for one day approximately every two weeks for five months following the NSS acquisition; this analysis includes two images per month from December 15, 2018, to April 30, 2019. Results illustrated in Fig. 14 found that the relative calibration approach improved image quality in all channels over time, a period that included multiple solar calibrations, which was consistent with the analysis shown above in Sec. 3.3–3.5. One exception is the results on March 31, 2019, in channel 4, which was due to the absence of clouds in the scene. As discussed earlier, the streaking metric in this situation does not accurately reflect the image quality. The consistent performance of the same set of relative gains over this period of time indicates stability in the relative detector response throughout the duration of this study. These results demonstrate a new on-orbit calibration strategy that was shown to produce consistent improvements to image quality in both the spatial domain and over time.

4 Conclusion

This work demonstrated the readiness of a new postlaunch calibration methodology in support of this generation of operational geostationary imagers, the GOES-R series ABI. The approach was

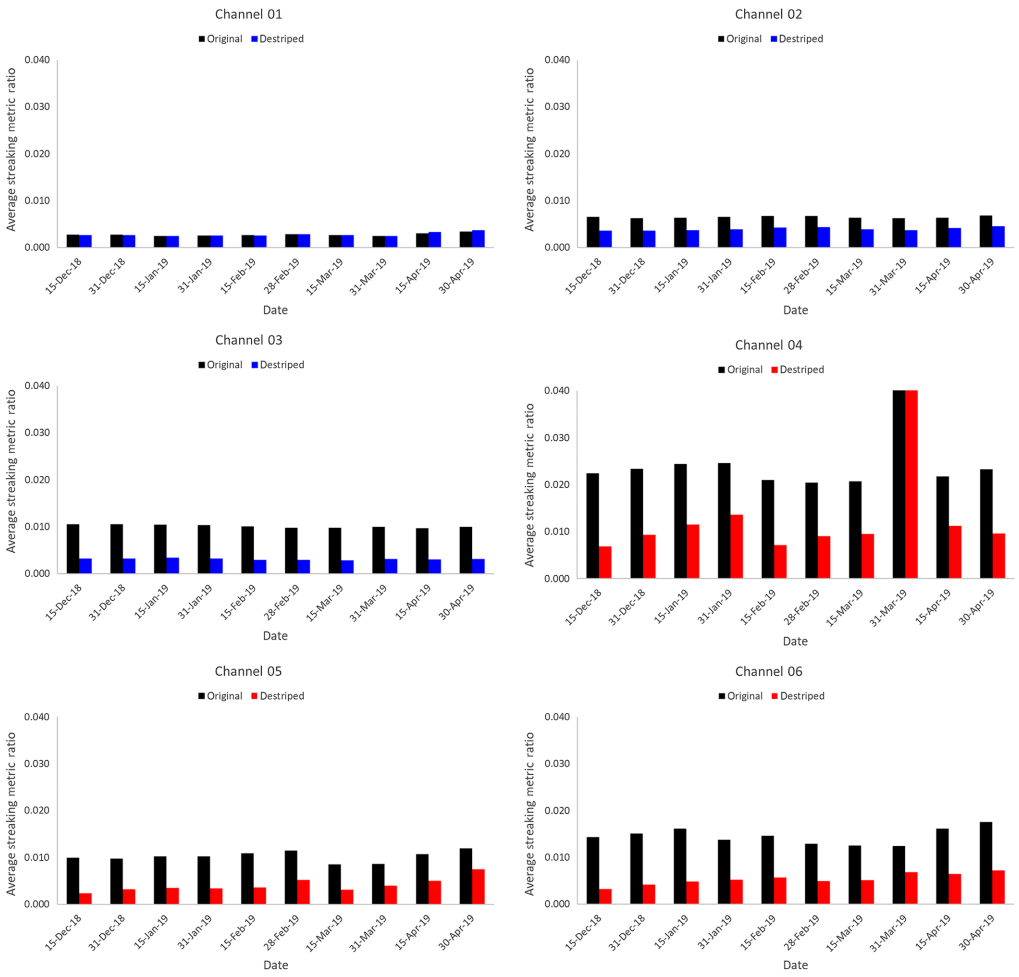

Fig. 14 Streaking metric results for the subset domain of one full disk image from GOES-17 ABI acquired at 2030 UTC for one day approximately every two weeks from December 15, 2018, to April 30, 2019. This illustrates the ability to successfully apply relative gains to scenes captured over an extended period of time.

found to improve image quality through the use of ABI special scans of uniform cloud targets and to provide consistent performance in space and time, both diurnally and over an extended period. This analysis leveraged previously established work and was conducted from December 2018 through April 2019, during which time visible image striping was impacting the image quality of the GOES-17 ABI RSB. The root cause of the GOES-17 ABI RSB striping was identified and addressed in May 2019 within the ground implementation, which removed the visible striping in the RSB from the operational data stream. Thus there was no longer a need to implement the NSS derived relative gains at that time. Both qualitative and quantitative analyses found that applying the optimal set of relative gains was equivalent to updating the operational data stream—further validating the approach and providing confidence for future use.

Operational implementation of this methodology could be invoked if necessary to remove persistent visible striping in the ABI RSBs. This method would be implemented in the same fashion as nominal calibration. The approach is only intended to be used as a last resort to improve the image quality of the operational data; implementation of this method does not preclude root cause evaluation, which would occur by processing L0 data offline. The relative calibration capability was fully tested and found to be easily implemented in the operational ground system (development environment) with only two lookup table changes required. Therefore, this postlaunch capability is available, if needed in the future, for all GOES-R ABI series of instruments to mitigate image quality impacts in support of ABI RSB L1b and L2+ based products. The required frequency to derive a new set of optimal relative gains is dependent upon the

stability and performance of each instrument; periodically collecting NSS data to maintain readiness for this method is an option, but it is not required. Timeline 25 collections with active tasking as described in Sec. 2.2 can easily be conducted to derive new data as needed.

Additionally, the developed approach could be used operationally as a back-up calibration methodology in the event of an on-board solar calibration failure—for example, a mechanical failure of the solar diffuser door. This relative calibration approach can be applied to improve image quality; absolute radiometric calibration of the instrument can be maintained with this method when used in combination with other postlaunch vicarious calibration methods, such as field campaigns and/or space-based intercomparisons with reference instruments.[11,12,15–18]

The application of the approach for the ABI TEB was investigated in support of GOES-17 ABI image quality improvements in response to a much larger effort to mitigate radiometric performance impacts from the GOES-17 thermal anomaly (loop heat pipe anomaly[19,20]) experienced on-orbit. NSS collections of uniform clouds and open ocean targets spanning a large range of radiance values were collected to investigate the translation of the strategy to image striping mitigation for the MWIR and LWIR focal planes. However, due to the temporal variation of the noise characteristics of the instrument, the approach was found to not improve image quality; the loop heat pipe anomaly is described in Refs. 19 and 20. Theoretically, the approach is valid for the TEB and remains an active area of research.

This state-of-the-art capability, specifically designed for the ABI, aligns the GOES-R program with the capabilities of other Earth observing large FPA systems. This methodology ensures a calibration strategy that is consistent with heritage approaches yet adapts to the new postlaunch validation challenges presented by the new class of operational imagers in the GOES-R series. The approach is ready for operational use, as needed, and can be easily implemented into operations to support the operational production of geostationary imagery of the Earth.

Acknowledgments

This work was funded by the GOES-R Program. The manuscript contents are solely the opinions of the authors and do not constitute a statement of policy, decision, or position on behalf of NASA, NOAA, or the U.S. Government. The authors would like to thank Dr. Daniel T. Lindsey and others in the GOES-R program for their contributions and support of this effort. The author has not identified any conflicts of interest.

References

1. S. Kalluri et al., "From photons to pixels: processing data from the advanced baseline imager," *Remote Sens.* **10**(2), 177 (2018).
2. "GOES-R series data book," Revision A. Prepared for National Aeronautics and Space Administration GOES-R Series Program Office, https://www.goes-r.gov/downloads/resources/documents/GOES-RSeriesDataBook.pdf (2019).
3. T. Schmit et al., "A closer look at the ABI on the GOES-R series," *Bull. Am. Meteor. Soc.* **98**(4), 681–698 (2016).
4. M. Weinreb et al., "Operational calibration of Geostationary Operational Environmental Satellite-8 and -9 imagers and sounders," *Appl. Opt.* **36**(27), 6895–6904 (1997).
5. F. Pesta et al., "Radiometric non-uniformity characterization and correction of Landsat 8 OLI using Earth imagery-based techniques," *Remote Sens.* **7**(1), 430–446 (2015).
6. A. Gerace et al., "Using DIRSIG to identify uniform sites and demonstrate the utility of the side-slither calibration technique for Landsat's new pushbroom instruments," *Proc. SPIE* **8390**, 83902A (2012).
7. B. Henderson and K. Krause, "Relative radiometric correction of QuickBird imagery using the side-slither technique on orbit," *Proc. SPIE* **5542**, 426–436 (2004).
8. F. Padula et al., "Introducing ABI North South scans for post-launch validation," in *Oral Presentation at 13th Annu. Symp. New Gener. Oper. Environ. Satell. Syst., Am. Meteorol. Soc. Annu. Meeting*, Seattle, Washington (2017).
9. C. Anderson et al., "Radiometric correction of RapidEye imagery using the on-orbit side-slither method," *Proc. SPIE* **8180**, 818008 (2011).

10. C. Chen, M. Wang, and J. Pan, "An improved side-slither method for on-orbit relative radiometric calibration," in *3rd Int. Symp. Space Opt. Instrum. and Appl., Springer Proc. Phys.*, H. Urbach and G. Zhang, Eds., Vol. 192, pp. pp. 351–359 (2017)
11. F. Padula et al., "Towards post-launch validation of GOES-R ABI SI traceability with high-altitude aircraft, small near surface UAS, and satellite reference measurements," *Proc. SPIE* **9972**, 99720V (2016).
12. B. Bartlett et al., "Independent validation of the advanced baseline imager (ABI) on NOAA's GOES-16: post-launch ABI airborne science field campaign results," *Proc. SPIE* **10764**, 107640H (2018).
13. J. Casey et al., "Characterization of GOES-16 ABI detector-level uniformity from post-launch North South scan collections of several earth targets," *Proc. SPIE* **10764**, 107640D (2018).
14. University of Wisconsin-Madison, "Space science and engineering, ABI quality score comparison," https://qcweb.ssec.wisc.edu/web/abi_quality_scores/ (2019).
15. J. McCorkel et al., "GOES-16 ABI solar reflective channel validation for earth science application," *Remote Sens. Environ.* **237**, 111438 (2020).
16. Committee on Earth Observation Satellites (CEOS) Working Group on Calibration and Validation (WGCV), "CEOS," 2020, http://ceos.org/ourwork/workinggroups/wgcv/.
17. Global Space-based Inter-Calibration System (GSICS), "GSICS," 2020, https://gsics.wmo.int/.
18. C. Cao et al., "Predicting simultaneous nadir overpasses among Polar-Orbiting Meteorological Satellites for the intersatellite calibration of radiometers," *J. Atmos. Ocean. Technol.* **21**, 537–542 (2004).
19. J. McCorkel et al., "GOES-17 advanced baseline imager performance recovery summary," in *Poster Presentation at IEEE Int. Geosci. and Remote Sens. Symp.*, Yokohama (2019).
20. F. Yu et al., "Radiometric calibration performance of GOES-17 advanced baseline imager (ABI)," *Proc. SPIE* **11127**, 111271C (2019).

Monica Cook received her BS degree and PhD in imaging science from the Rochester Institute of Technology in 2010 and 2014, respectively. She is a systems engineer at GeoThinkTank, LLC, an imaging science and geospatial services company based in Washington, DC. She is currently supporting the GOES-R Program at NASA Goddard Space Flight Center. Her current research interests include on-orbit calibration/validation for geostationary instruments and remote sensing based science applications.

Biographies of the other authors are not available.